Hindawi
Shock and Vibration
Volume 2019, Article ID 8526179, 16 pages
https://doi.org/10.1155/2019/8526179

Research Article

Adaptive Damping of a Double-Beam Structure Based on Magnetorheological Elastomer

Tomasz Szmidt,[1] Dominik Pisarski,[1] Robert Konowrocki,[1] Stefan Awietjan,[2] and Anna Boczkowska[2]

[1]*Institute of Fundamental Technological Research, Polish Academy of Sciences, Pawińskiego 5b, 02-106 Warsaw, Poland*
[2]*Faculty of Materials Science and Engineering, Warsaw University of Technology, Wołoska 141, 02-507 Warsaw, Poland*

Correspondence should be addressed to Robert Konowrocki; rkonow@ippt.gov.pl

Received 29 October 2018; Revised 25 January 2019; Accepted 11 February 2019; Published 25 March 2019

Academic Editor: Luca Landi

A method of vibration reduction based on activation of an MRE block that couples twin cantilever beams at their free ends is investigated. Four types of magnetorheological elastomers have been manufactured, and their rheological properties in a range of magnetic field intensities are established. Free vibrations of several double-beam structures with controllable damping members made of these MREs are investigated, and a method of semiactive control of such structures is proposed. The effects of compression of the elastomers and alignment of the magnets used to activate them are reported. The mathematical modeling of the system is verified experimentally.

1. Introduction

Systems of two parallel elastic continua are used in various devices and mechanical, civil, or aircraft structures. Examples include aircraft wing spars, bridge spans, and linear guideways used in plotters or in some technological processes. In these systems, a soft viscoelastic layer or patch may be placed between two rigid facesheets to ensure efficient vibration suppression.

Basically, there are two methods to dissipate mechanical energy in such systems. When the initial conditions imposed on both beams are not the same or when the beams have different masses (stiffnesses), one may exploit the relative transverse motion of the beams, which leads to an axial deformation of the viscoelastic element placed between them. However, the beams eventually synchronize their motion, and this way of damping becomes ineffective—the same as in the case of identical beams and initial conditions [1]. Then, the shear deformation of the soft middle layer becomes the predominant mechanism of energy dissipation in a sandwich beam [2–7].

In order to control these vibrations, smart materials can be used in the soft middle layer. Magnetorheological elastomers (MREs) are composite materials that are considered to be smart materials [8]. Solid-state MREs overcome drawbacks of MR fluids, such as the leakage of the liquid and sedimentation of the particles. They are classified as intelligent materials well suited for providing effective structural control. They possess tunable rheological properties and can be used in adaptive structures for aerospace [9], automotive [10, 11], railway [12, 13], civil [14], and electrical engineering applications for linear and rotational motion and vibration control [15, 16].

Magnetorheological elastomers exhibit interesting mechanical properties. These materials change their rheological properties under an applied external magnetic field. This behavior is similar to magnetorheological fluids, but MREs are their solid equivalents. In magnetorheological elastomers, magnetoactive particles (e.g., iron and cobalt) are embedded within an elastic polymer matrix [17]. The matrix enables relatively high strains and maintains the overall shape of the element. The magnetorheological effect is based on dipole interactions between ferromagnetic particles [18]. Under a magnetic field, the particles tend to align themselves in parallel with the lines of the magnetic field [19]. Due to their rapid response [20, 21], the elastic moduli of these flexible smart composites can be effectively controlled in

almost real-time according to varying external excitations. Thus, the MREs provide greater potential for vibration suppression in an active manner in a wider range of frequencies [22–24].

This tendency has been used to obtain several magnetorheological elastomers with aligned chain-like microstructures. The polymer matrix preserves the alignment of the particles after a curing process. From our previous research [25], it is known that in MR composites, an aligned microstructure provides a significantly greater magnetorheological effect than an isotropic arrangement of the particles [26, 27]. To manufacture the magnetorheological elastomers considered in our investigations described in the paper, we followed the methods of Boczkowska et al. [28]. Applying this method, it has been found that the rheological properties strongly depend on the MRE microstructure, in particular on the size/shape of the particles and their arrangement. By optimizing the particles' size, shape, and alignment, the stiffness of the MREs under an applied magnetic field has been increased.

The application of magnetorheological materials to the mitigation of the vibrations of sandwich beams is a relatively new idea. These materials can be placed along the entire length of the system in the form of an adaptive viscoelastic core [29, 30], as a single patch [31], or as several patches [32]. The dynamics of these systems when subjected to various excitations has been investigated quite thoroughly, both experimentally and theoretically [33, 34]. The aforementioned studies are related to passive methods of vibration reduction of double-beam structures, which are not always sufficiently effective.

In addition to beam structures, MREs can be used in plate systems. Yeh [35] presented a vibration analysis of a rectangular sandwich plate composed of an MRE core layer and a constraining layer. The MR material exhibited a significant effect on the vibrational characteristics of the plate and a rapid time response. Vemuluri et al. [24] studied the dynamic performance of a tapered sandwich plate partially treated with an MRE layer. The laminated composite plate with an MR fluid was investigated by Ramamoorthy et al. [36]. de Souza Eloy et al. [22] investigated numerically and experimentally sandwich panels with carbon/epoxy composite skins and a magnetorheological elastomer (MRE) honeycomb core. The obtained experimental results showed good performance in the attenuation of the vibration level, especially the fundamental vibration mode of the structure. The magnetic field applied on the free end of the test panel was able to reduce significantly its first natural frequency value.

Few of these works tackle the problem of the semiactive control of such systems using magnetorheological materials. Ndemanou et al. independently proposed a method based on the Lyapunov stability theory [37, 38]. Namely, the controller aims at the maximization of the instantaneous energy dissipation of the system. In the first of these works, a double-beam structure is stabilized through the relative transverse motion of the beams, which leads to an axial deformation of a controllable MR damper. In the second, the shear deformation of several damping blocks made of an MRE is exploited. In another approach based on the latter mechanism, the linear quadratic regulator was applied [39].

These studies are confined to numerical simulations of semiactively controlled systems. For example, Rajamohan et al. claim that "the implementation of the controller, however, would require further developments in compact electromagnets to apply the controlled magnetic field on the surfaces of the treated structures" [39]. Indeed, in most of the studies, the electromagnetic devices were placed near the vibrating structure to control the rheological properties of the material [3, 6]. However, such an approach requires large and heavy machinery built around the system, which may be cumbersome. Moreover, attracting the MRE by external magnets causes the effect of negative stiffness, which is in general undesirable. As far as the knowledge of the present authors extends, the research [40] is the only one in which the electromagnets were attached directly to the vibrating structure. This study showed a rather mediocre performance of the control in the system with classical electromagnets and a damping block made of an isotropic MRE.

The rest of this paper is structured as follows. Four types of magnetorheological elastomers of have been manufactured. Their rheological properties in a range of magnetic field intensities have been established, and the free vibrations of several double-beam structures with damping blocks made of these materials are investigated. Permanent magnets are then used to identify a type of MRE, providing decent damping capabilities. Apart from the increased shear stiffness and damping, additional phenomena that affect the performance of the method are reported. A dynamic model of the system is presented and used to validate a stabilizing semiactive control strategy. Finally, the theoretical findings are verified experimentally.

2. Fabrication and Rheological Properties of the MRE Samples

Two types of elastomer matrices were used to produce the MRE samples, referred to as PU 70/30 and U1440. The PU 70/30 is a soft polyether-based polyurethane that is obtained from two polyether polyols: 14922 and VORALUX® HF 505 (in weight ratio 70 : 30) in a mixture with the isocyanate compound HB 6013, supplied by the Dow Chemical Company. The second matrix, referred to as U1440, was synthesized using the two-component polyurethane elastomer Biresin® U1404, supplied by SIKA. The elastomer was produced by a reaction of isocyanate prepolymer resin and amine hardener in 80 : 100 weight ratio.

In both cases, the mixing of the substrates and the curing process were conducted at room temperature. The PU 70/30 polyurethane is characterized by a low density (1.03 g/cm^3), low viscosity before curing (ca. 1600 mPa·s), and low hardness (below 10°ShA). The U1440 polyurethane is also characterized by a low density (1.05 g/cm^3), relatively low viscosity before curing (ca. 3000 mPa·s), and a hardness (40°ShA) four times higher than that of PU 70/30. These properties allow us to obtain a relatively high magnetorheological effect in the composites based on both types of

matrices. The relatively low viscosity during the processing of the MRE makes it easy to obtain an alignment of the particles under an external magnetic field.

Carbonyl iron powder, produced by Fluka, was used for the magnetoactive particles for the fabrication of the samples. The particles are spherical, and their average diameter is 6–9 μm. Two volume shares of the carbonyl iron particles were used. The first was 11.5 vol.%. In our previous studies [41], we obtained the highest magnetorheological effect for this amount of particles. The second amount was equal to 33 vol.%. The samples were subjected to a magnetic field during curing to obtain aligned iron particle chains within the elastomer. A magnetic field strength of 240 kA/m was used.

The characteristics of all the MRE samples are given in Table 1.

The rheological measurements were carried out using an ARES rheometer from TA Instruments under a preselected magnetic field (Figure 1). The plate-plate system with diameters of 20 mm and with a 2 mm gap between plates was used. The magnetic field was varied over the range 0–320 kA/m. The experiments were conducted at an ambient temperature of 25°C. The excitation was applied in a sinusoidal form with angular frequency $\omega = 19.9$ rad/s and at constant strain of 0.1%.

MR elastomers are normally operated with small deformations in the preyield regime of the linear viscoelastic region. They are intended to be used as structural materials in applications where the load is often dynamic. Under a cyclic dynamic loading, the material deforms and returns to its original form during one cycle. In viscoelastic materials, some part of the deformation energy input is stored and recovered during each cycle and some is dissipated as heat. The storage modulus, $G\prime$, represents the ability of the viscoelastic material to store the energy of deformation, which contributes to the material's stiffness. The loss modulus, G'', represents the ability of the material to dissipate the energy of deformation.

In this study, both the elastic (storage) modulus and the loss modulus were measured as functions of the magnetic field at room temperature. As shown in Figure 2, the storage modulus increases significantly with the strength of the applied magnetic field for all samples. However, this growth strongly depends on the matrix material and the amount of particles within the matrix. The change of the modulus under a magnetic field is called the magnetorheological effect. The magnetorheological effect can be expressed by the relative change of the elastic modulus $\Delta G\prime/G_0'$ under the magnetic field. This effect can be used for variable stiffness devices because it is fully reversible. It is related to the tendency of the composites to attain the minimal energy. The soft matrix enables some elastic displacement of the particles. However, such displacements generate a strain in the matrix and a stress. As a result, the material's properties are changed. The softer matrix PU 70/30 exhibited a larger MR effect than U1404 due to larger strengthening effect of the particles under the magnetic field.

The same conclusions regarding the behavior of the elastomers under the magnetic field can be drawn for the loss modulus (see Figure 3).

Table 1: Characterization of fabricated MRE samples.

Sample	Polymer matrix	Particles content	Density	Magnetic field during curing
1A	PU 70/30	11.5 vol.% Fe	1.82 g/cm^3	240 kA/m
1B	PU 70/30	33 vol.% Fe	3.28 g/cm^3	240 kA/m
2A	U1404	11.5 vol.% Fe	1.83 g/cm^3	240 kA/m
2B	U1404	33 vol.% Fe	3.30 g/cm^3	240 kA/m

During our experiments with a passively activated double-beam structure, the values of the magnetic field measured in the centers of damping elements amounted to 103, 159, and 263 kA/m, respectively, with all three types of magnets used in the study, and without the brass plate. The brass plate was intended to prevent compression of the elastomers (see Section 5.4). When the brass plate was inserted, the intensity dropped by approximately 8 kA/m.

3. Dynamic Model

This section describes the mathematical model of the system which will by used for development of the control strategy. It is based on the model already presented and verified experimentally [42], which was further simplified in [1].

The double-beam structure to be investigated is presented in Figure 4. It consists of two elastic facesheets coupled at their free ends by a smart damping element made of MRE. To prevent buckling of the structure, a distance roll modeled as a linear spring of a very high stiffness k is placed between the beams at a distance ξ_k. Both beams have length L, width b, thickness d, and mass per unit length ρS and are mounted in a clamped support.

We will study the vibrations of the structure in the plane of symmetry $\xi - \eta$. The displacements of the beams from their equilibria in the η-direction are denoted by $w_{1,2}(\xi, t)$. The beams are slender, and their deflections are small, so the linear Bernoulli–Euler beam theory is valid. The external damping of the beams is neglected. The effect of gravity, which acts perpendicularly to the plane of vibrations, is also not taken into account.

The damping block has a rectangular shape $2a \times b \times 2h$ and mass 2 M. Its center is located at a distance of $\xi = L - a$ from the support. The rheological parameters of this element are controlled using electromagnetic devices, which are attached at the tip of the structure and have a total mass of M_a. The constitutive law of the MRE in a dynamic test can be written in the following form:

$$\tau = G'\varphi + \frac{G''}{\omega}\dot{\varphi}, \tag{1}$$

where τ is the shear stress, $\varphi = \varphi(t)$ is the angle of shear deformation, and $G' = G'(u, \omega)$ and $G'' = G''(u, \omega)$ are the storage and loss moduli. Both these parameters are functions of the applied magnetic field u and the frequency of angular deformation ω. However, a typical change of storage or loss modulus due to the applied magnetic field yields only a slight change in this frequency. The values of G' and G'' are nearly constant within such a narrow range of ω, so we may treat the values of both rheological parameters as independent of it.

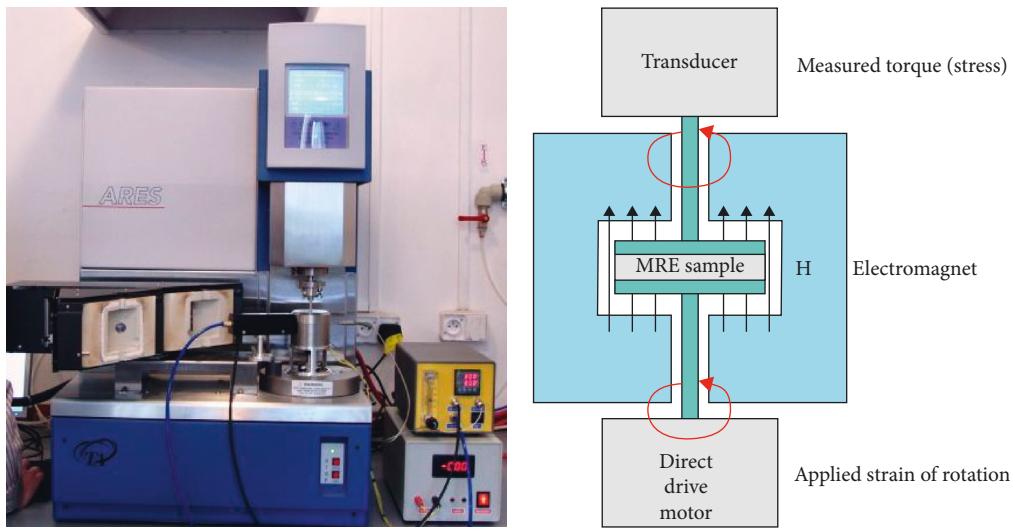

Figure 1: ARES rheometer with magnetic coil device and measurement scheme.

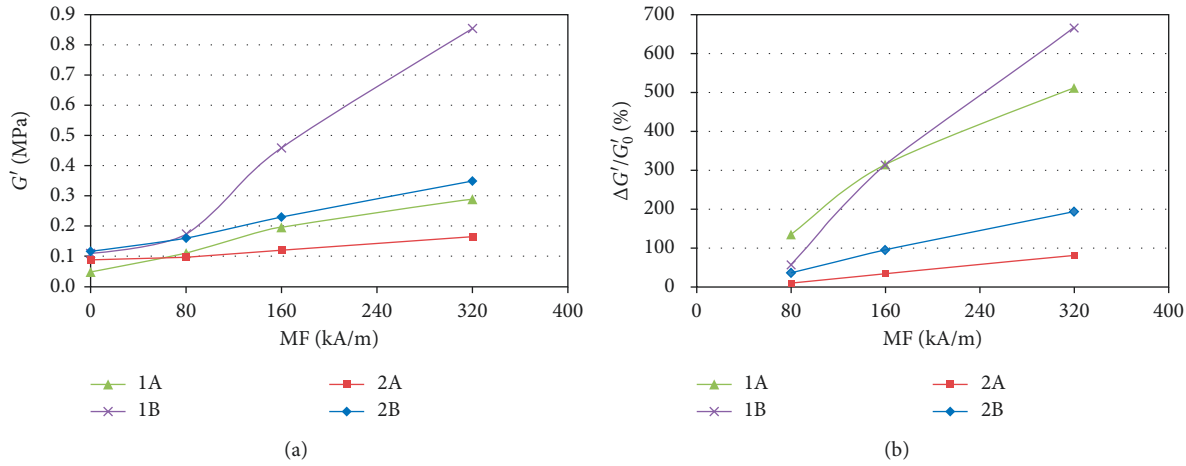

Figure 2: Storage modulus G' and relative MR effect for samples under different magnetic field strengths.

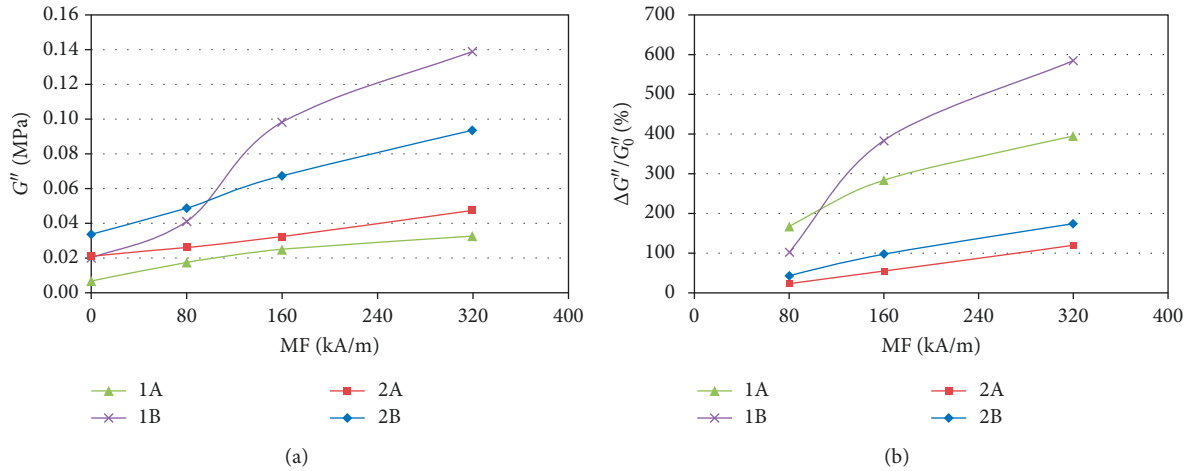

Figure 3: Loss modulus G'' and relative MR effect for samples under different magnetic field strengths.

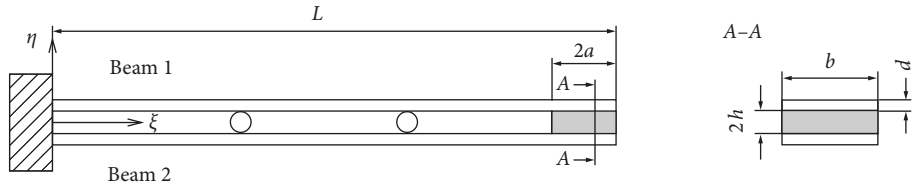

Figure 4: Double-beam structure with embedded intelligent damping MRE element.

Moreover, the external devices are only able to control the rheological parameters in a limited range, where linear approximations are justified. Thus, we can write

$$G' = (1 + r_1 u) G_0', \qquad G'' = (1 + r_2 u) G_0'', \tag{2}$$

where $u \in [0, 1]$ is the normalized value of the magnetic field intensity, G_0' and G_0'' are the storage and loss modulus without any magnetic field applied, and r_1 and r_2 are positive constants determined experimentally.

The shear deformation of the damping element yields bending moments as well as axial forces acting on both beams. Moreover, the relative motion of the beams generates transverse forces. Having assumed that the block is not too long ($2a \ll L$) and treating the parts of the beams over the damping block as rigid bodies, we may reduce the forces to the pole, which is the point over the center of the block (see Figure 5).

We now present the formulas for the bending moments and forces acting on Beam 1, which have been developed using the truss model proposed in [42]. Assume that the angles of deflection of the beams at the point $\xi = L - a$ are the same and equal to $\varphi = (\partial w/\partial \xi)(L - a, t)$ and the relative displacements of the beams at this point are $\Delta w = w_1(L - a, t) - w_2(L - a, t)$. We then have the following expressions.

For the bending moment $\mathscr{M}$,

$$\mathscr{M} = 2abh\left(G'\varphi + \frac{G''}{\omega}\dot{\varphi}\right), \tag{3}$$

transverse force $\mathscr{F}$,

$$\mathscr{F} = -\frac{bh}{a}\left(G'\Delta w + \frac{G''}{\omega}\Delta\dot{w}\right), \tag{4}$$

and axial forces $\mathscr{N}$,

$$\mathscr{N} = -2ab\left(G'\varphi + \frac{G''}{\omega}\dot{\varphi}\right). \tag{5}$$

The influence of the axial force appears to be of minor importance and will be disregarded. This is mainly because the axial forces act in opposite directions (i.e., when Beam 1 is compressed, Beam 2 is stretched) and partly because these forces are too small to disturb the dynamics of the rigid facesheets. With this simplification, we end up with a linear dynamical model in the form of the following system of coupled partial differential equations governing the dynamics of both beams:

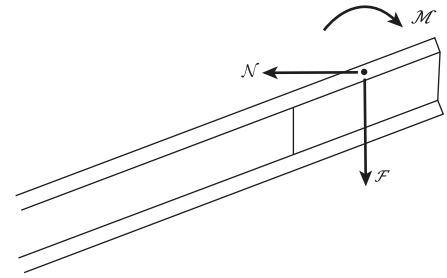

Figure 5: Forces generated by the damping block reduced to the pole.

$$\left(\rho S + \left(\mathscr{M} + \frac{1}{2}\mathscr{M}_a\right)\delta_{L-a}\right)\frac{\partial^2 w_{1,2}}{\partial t^2} + EI\frac{\partial^4 w_{1,2}}{\partial \xi^4} + E^* I\frac{\partial^5 w_{1,2}}{\partial \xi^4 \partial t} = \mathscr{M}\frac{d}{d\xi}\delta_{L-a} \pm \mathscr{F}\delta_{L-a}, \tag{6}$$

where $\mathscr{M}$ and $\mathscr{F}$ are given by formulas (3) and (4), δ_{L-a} is Dirac's delta at $\xi = L - a$, and $(d/d\xi)\delta_{L-a}$ is the unit doublet at $\xi = L - a$. Note that the positive sign of the transverse force $\mathscr{F}$ corresponds to beam 1, and the negative sign corresponds to the other beam.

To develop a control strategy, we need to introduce an energy-related function. The most natural choice for this function, which also turns out to be effective, is to define V as a function related to the total mechanical energy of the system, similar to [1]. We neglect the kinetic energy of rotation of the damping element and the kinetic energy of its shear deformation because they make only a minor contribution to the total mechanical energy of the system. After some calculations, we obtain the following formulas:

(1) The combined kinetic energy of the damping element and the actuator:

$$V_k^{\text{element}} = \frac{1}{2}\sum_{i=1}^{2}\left(\mathscr{M} + \frac{1}{2}\mathscr{M}_a\right)\frac{\partial w_i}{\partial t}(L - a, t)^2. \tag{7}$$

(2) The elastic strain energy of the damping element (note that $(\partial w_1/\partial \xi)(L - a, t) = (\partial w_2/\partial \xi)(L - a, t)$ by assumption):

$$V_e^{\text{element}} = \frac{1}{2}\cdot 2abG'\frac{\partial w_1}{\partial \xi}(L - a, t)^2. \tag{8}$$

(3) The kinetic energy of the beams:

$$V_k^{\text{beam}} = \sum_{i=1}^{2}\int_0^L \frac{1}{2}\rho S\left(\frac{\partial w_i}{\partial t}(\xi, t)\right)^2 d\xi. \tag{9}$$

(4) The elastic strain energy of the beams:

$$V_e^{\text{beam}} = \sum_{i=1}^{2} \int_0^L \frac{1}{2} EI \left(\frac{\partial^2 w_i}{\partial \xi^2} (\xi, t) \right)^2 d\xi. \tag{10}$$

Therefore, the energy function, closely related to the total mechanical energy of the system, is given by the following equation:

$$V = V_k^{\text{element}} + V_p^{\text{element}} + V_k^{\text{beam}} + V_p^{\text{beam}}. \tag{11}$$

We are going to analyze the approximate solution to the partial equations governing the system in the form of a linear combination of cantilever beam eigenfunctions:

$$w_{1,2}(\xi, t) = \sum_{i=1}^{n} W_i(\xi) T_i^{(1,2)}(t), \tag{12}$$

$$W_i(\xi) = C_i \left[\cosh \frac{\lambda_i}{L} \xi - \cos \frac{\lambda_i}{L} \xi + \frac{\sin \lambda_i - \sinh \lambda_i}{\cos \lambda_i + \cosh \lambda_i} \left(\sinh \frac{\lambda_i}{L} \xi - \sin \frac{\lambda_i}{L} \xi \right) \right], \tag{13}$$

where λ_i are the roots of the characteristic equation $\cos \lambda \cosh \lambda = -1$, and C_i are the constants which normalize the mode shapes with respect to the norm induced by the scalar product $\int_0^L W_i(\xi) W_j(\xi) d\xi$. Applying Galerkin's procedure, we obtain a set of $2n$ second-order ordinary equations for the vectors of generalized coordinates $\mathbf{T}^1 = [T_1^1, \ldots, T_n^1]^{\mathrm{T}}$ and $\mathbf{T}^2 = [T_1^2, \ldots, T_n^2]^{\mathrm{T}}$. We then reduce the order of the problem by substituting $x_i = T_i^1, x_{n+i} = T_i^2, x_{2n+i} = \dot{T}_i^1, x_{3n+i} = \dot{T}_i^2 (i = 1, \ldots, n)$. This leads to the following normal form of the set of $4n$ ordinary differential equations governing the dynamics:

$$\dot{\mathbf{x}}(t) = \mathbf{A}\mathbf{x}(t) + u(t)\mathbf{B}\mathbf{x}(t), \quad \mathbf{x}(0) = \mathbf{x}_0. \tag{14}$$

For the set of admissible controls, we assume

$$u(t) \in \mathcal{U} = [u_{\min}, u_{\max}], u_{\min} \geq 0, u_{\max} > u_{\min}. \tag{15}$$

Following [42], eight basis functions appear to be sufficient to obtain the desired precision for the approximation.

The energy function (11) for the discrete system (14) can be written as a quadratic function of the state variables as follows:

$$V = \frac{1}{2} \mathbf{x}^{\mathrm{T}} \mathbf{Q} \mathbf{x}, \tag{16}$$

where the energy matrix is a function of the control variable, i.e., $\mathbf{Q} = \mathbf{Q}(u)$. However, we have found that $\mathbf{Q}$ can be treated as independent of u. Thus, we assume $\mathbf{Q} = \mathbf{Q}(1) = \text{const}$.

4. Semiactive Control Strategy

We will now study the stabilization of the semiactive system (14) with respect to perturbations of the initial state $\mathbf{x}_0$. The problem of stabilization consists in choosing a feedback control function $u \in \mathcal{U}$ such that the solution $\mathbf{x}$ of the resulting feedback system associated to (14) converges in some sense to the equilibrium state $\mathbf{x}_0$ within a suitable length of time. For the controller, we shall employ the method proposed in [1, 43]. The selection of this method is motivated by the good balance it strikes between the performance of the controller and its practical simplicity. It has been validated numerically that the method achieves a fair performance in stabilizing impulse-excited vibrations. By relying on a time-invariant state-feedback switching control law, the method can be successfully implemented using a system of displacement sensors, a signal amplifier, and a PC equipped with an analog I/O card. For the convenience of the reader, we summarize the underlying principles of the method in the following. The aim is to design a control $u^*(t) \in \mathcal{U}$ that provides the best instantaneous dissipation of the energy V as defined in (16). Therefore, we require the following equation:

$$\text{for every time } t : u^*(t) = \text{argmin}_{u \in \mathcal{U}} \dot{V}(\mathbf{x}(t)). \tag{17}$$

Note that,

$$\dot{V}(\mathbf{x}(t)) = \frac{1}{2} \dot{\mathbf{x}}^{\mathrm{T}}(t) \mathbf{Q} \mathbf{x}(t) + \frac{1}{2} \mathbf{x}^{\mathrm{T}}(t) \mathbf{Q} \dot{\mathbf{x}}(t). \tag{18}$$

By using $\mathbf{Q} = \mathbf{Q}^{\mathrm{T}}$, the insertion of the governing equations (14)–(18) yields

$$\dot{V}(\mathbf{x}(t)) = \mathbf{x}^{\mathrm{T}}(t) \mathbf{Q} \mathbf{A} \mathbf{x}(t) + u \mathbf{x}^{\mathrm{T}}(t) \mathbf{Q} \mathbf{B} \mathbf{x}(t). \tag{19}$$

From (15) and (19), it follows that the solution to the problem (17) is given by the following equation:

$$u^*(t) = \begin{cases} u_{\max}, & \text{if } \mathbf{x}^{\mathrm{T}}(t) \mathbf{Q} \mathbf{B} \mathbf{x}(t) < 0, \\ u_{\min}, & \text{otherwise.} \end{cases} \tag{20}$$

It should be noted that the internal structural damping guarantees that $\mathbf{A}$ is a Hurwitz matrix (i.e., every eigenvalue of $\mathbf{A}$ has strictly negative real part). Assuming the following bounds on the admissible control $u_{\min} = 0$, $u_{\max} > 0$, we can then see from $\mathbf{Q} > 0$ and (19) that the control law given by (20) guarantees a permanent decrease of the global system energy $\dot{V} < 0$, and thus the asymptotic stability of (14).

5. Experimental Assessment of the Performance of MREs in a Passively Activated System

5.1. Test Stand. As the real object of investigation, we consider a two-beam structure imitating structural elements such as aircraft wing spars, cranes, bridge spans, pipelines, and rail plotters. A photograph of the entire laboratory setup is shown in Figure 6, a schematic in Figure 4, and the fundamental parameters of this test rig in Table 2.

The system was made of steel beams, each having nominal length $L = 0.8$ m and cross-sectional area $S = 0.00003\,\text{m}^2$ ($0.015\,\text{m} \times 0.002\,\text{m}$). The steel material was chosen because of its ferromagnetic properties, which

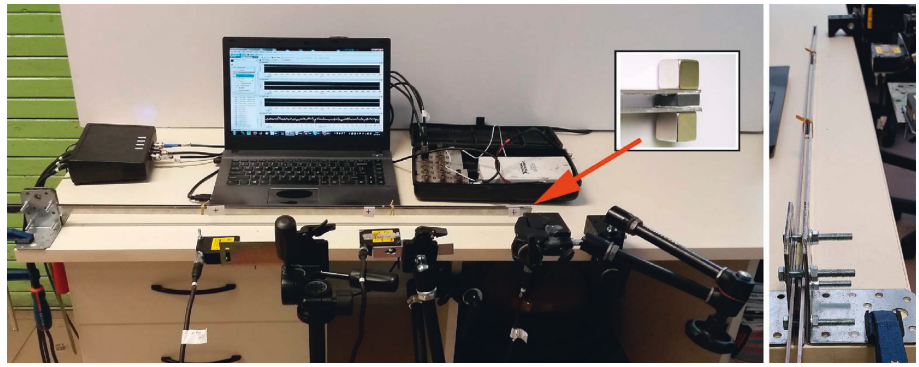

Figure 6: Laboratory two-beam construction system with MR elastomer damper.

Table 2: Fundamental parameters of the test rig.

Parameter	Value
Dimensions of a single beam	$L = 800$, $b = 15$, $d = 2$ mm
Position of distance rolls from the support	$x_1 = 247$, $x_2 = 546$ mm
Position of sensors from the support	$S_1 = 260, S_2 = 520, S_3 = 770$ mm
Dimensions of MRE blocks	$2a = 16$, $b = 15$, $2h = 6$ mm
Resolution/response time of sensors	0.01 mm/ < 900 μs
Sampling of the measurement card	1000 Hz
Initial deflection of the beam at sensor S_3	32 mm

allowed us to obtain the highest magnetic field intensity. The free ends of the beams were coupled by a rectangular block made of one of the MREs that were described in Section 2. The damping element was glued using an MS-polymer adhesive.

The assembly of the MRE element in the investigated system allowed for an easy change of the magnetic flux by using various permanent magnets attached at the end of the structure. The basic parameters for the NdFeB magnets used in the investigation are presented in Table 3.

The magnets were stuck by the magnetic force generated between them and the facesheets. One of the magnets faced its north pole towards the beam while the polarization of the other one was the reverse. Consequently, the magnetic field within the damping element was as uniform as possible, and the passive action of the magnets increased both the shear stiffness and damping properties of the elastomers. This allowed a passive-adaptive damping of the structure.

The shear deformation of the damping member generates axial forces, which may produce buckling of the beam that is compressed. This complicates the measurements and analyses of the effect in which we are actually interested. To keep the gap between the beams constant over their lengths, two lightweight rolls were placed at distances of $x_1 = 0.247$ m and $x_2 = 0.546$ m from the support. The beams were tightened to the distance rolls by thin and light rubber bands. The rolls were made of aluminum tubes, so the rolling drag would be as small as possible.

Table 3: Neodymium Iron Boron magnets used in the investigation.

Parameter	M5	M8	M15
Cross-sectional area		15 mm × 15 mm	
NdFeB material	N38	N38	N42
Thickness	5 mm	8 mm	15 mm
Mass	8.4 g	13.5 g	25 g

The structure was fixed to a solid workshop table in a clamped configuration with two steel mounting brackets. The oscillatory motion of the coupled two-beam system was realized by a lateral deflection in the (horizontal) y-direction. The plane of motion was perpendicular to the force of gravity, thus the effect of gravity could be neglected. To arrive at a precise measurement of the horizontal deflection, Baumer-OADM 12I6430/S35A laser distance sensors were used. The laser sensors provided a maximum measurement resolution of 0.01 mm in less than 900 μs. Because the measurement range of the laser sensors was within the 30–130 mm interval, they were mounted near the beams at three points, marked by S_1, S_2, and S_3 in Figure 4. Because these sensors realized a contactless and perturbation-free signal registration, their operation did not reduce the accuracy of the remaining measurement systems in the considered setup, as confirmed in [44, 45]. During the tests, an NI USB-6218 analog-digital converter was used for data acquisition. All of the signals from the laser sensors were recorded by means of this converter with a sampling frequency of 1000 Hz.

The experiments were conducted according to the scheme (1A, 1B, 2A, 2B) × (thick, thin) × (no magnet, M5, M8, M15) × (compression, no compression) × (trial 1, trial 2), which resulted in 128 experimental scenarios. For the thin beam (4 mm thickness of the damping member), the results were qualitatively the same as for the thick beam ($2h = 6$ mm), yet quantitatively in most scenarios they are less pronounced and, therefore, they will be disregarded in this article. However, when analyzing the effect of the alignment of the magnets, the results obtained for the thin beam are easier to see, so some of them are going to be presented in Section 5.5.

The effect of the compression of the elastomer by the forces generated by the magnets is inherently present in the

system, and for the purpose of analysis, it was excluded by inserting a brass distance plate near the damping block (see Section 5.4 for details).

Two trials were performed to ensure that the results would be repeatable. Apart from a few trials when random accidents happened (such as a detachment of the sticker at which the laser sensor was aimed), the experiments were actually perfectly repeatable and, therefore, only the results for single trials will be presented.

Each trial was initiated by a deflection of the system with zero initial velocity. After releasing the structure, the vanishing free vibrations of the first mode were recorded. The excessive amount of data was reduced by taking averages of the subsequent blocks of five observations. Examples of time series for a trial for the thick beam, with damping member made of elastomer 1B, under the action of magnets M8, and with the effect of compression (no brass plate), are shown in Figure 7.

5.2. Experimentally Observed Vibration Period and Damping. The experiments with free vibrations will be analyzed in this section. The oscillations at the first natural frequency were induced. The consecutive minimal and maximal beam deflections w_i and the points t_i of time at which they occur were determined fully automatically by local approximations of the time series with quartic polynomials. The extremes were calculated until the amplitude of the vibrations decreased to the threshold when the signal-to-noise ratio became too low, which happened when the amplitude measured by sensor S_3 was 2 mm. An example of the time response with calculated extremes is shown in Figure 8.

To investigate the character of the vibrations, doubled times of increase and decrease τ_i and logarithmic damping decrements δ_i corresponding to consecutive extreme deflections were calculated:

$$\tau_i = 2\left(t_{i+1} - t_i\right),$$
$$\delta_i = \ln \frac{\left|w_{i+1} - w_i\right|}{\left|w_{i+3} - w_{i+2}\right|}. \tag{21}$$

No differences were observed between the times of decrease and the times of increase; so, τ_i is the estimator of the period of the vibrations. The values of the period and the decrement for consecutive cycles are shown in Figures 9 and 10.

For a classical harmonic oscillator with viscous damping, the series τ_i and δ_i are constant. Thus, the amplitude of the vibrations decreases at a constant rate, making the oscillations vanish exponentially. In the analyzed system, this is satisfied quite well in most of the analyzed scenarios. In the case of the beam with a damping member made of MRE 1B and subjected to the action of the biggest magnets, a nonlinear behavior of the material can be observed because the vibrations of high amplitudes have longer periods, and their suppression is less pronounced.

The attachment of magnets generally increases the period of vibrations because of the additional inertia introduced to the system. Moreover, the damping becomes more pronounced. To analyze these effects, an analysis analogous to the one from the previous subsection was conducted. With no magnets, the average period of vibrations is 0.390, 0.373, 0.351, and 0.324, respectively, for MRE 1A, 1B, 2A, and 2B. The logarithmic damping decrement is 0.038, 0.108, 0.067, and 0.123. The damping ratio (the quotient of the decrement and the period) is 0.097, 0.289, 0.190, and 0.378 (1/s). These values are much higher than those theoretically predicted because structural damping is present in the real system, yet it is neglected in the model.

We will now move on to the empirical analysis of the magnetorheological effect on vibrations (Figure 11). The action of the magnets increases the stiffness of the damping members. The relative growth of the average vibration period is both qualitatively and quantitatively in good agreement with the theoretical predictions. For the damping (both the average decrement and the damping factor), the results are a little different. The relative growth of damping under the action of the magnets is lower than predicted by the model. In the real system, the energy dissipates not only through the damping member but also inside the beams, through the support, and in the form of aerodynamic drag and rolling friction of the distance rolls. This structural and material damping is difficult to quantify, and it partly overshadows the magnetorheological effect. However, it yields results that are more realistic because many sources of damping are inherently present in all engineering structures.

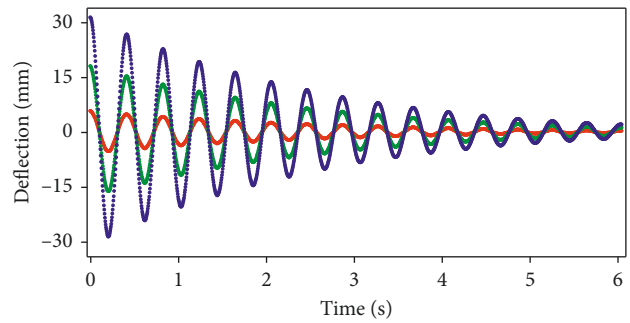

Figure 7: Empirical deflection of the system measured by sensors S_1 (red), S_2 (green), S_3 and (blue); MRE 1B, magnet M8, compression.

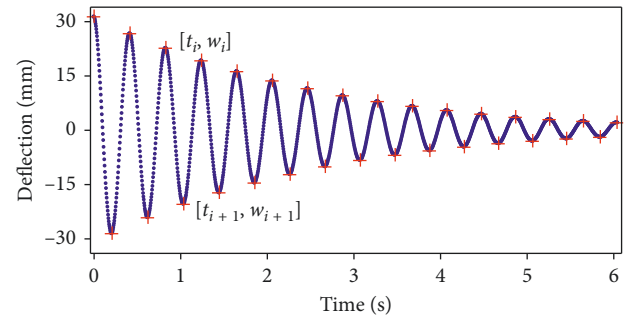

Figure 8: Vibrations measured by sensor S_3 with calculated extremes; MRE 1B, magnet M8, compression.

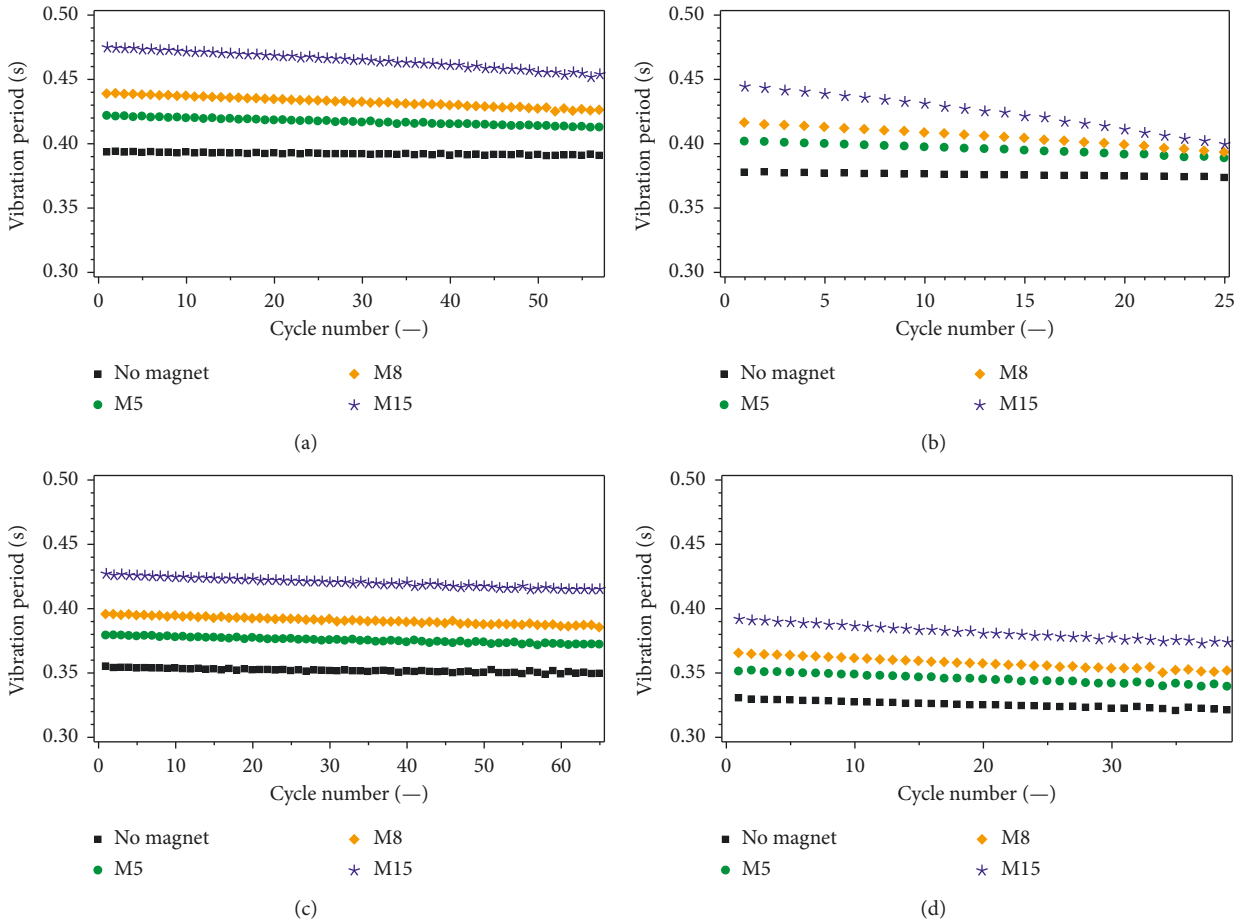

Figure 9: Vibration period of subsequent cycles: (a) MRE 1A, (b) MRE 1B, (c) S_3MRE 2A, and (d) MRE 2B, compression.

The relative growth of the damping is much higher for both elastomers based on the PU 70/30 matrix, which confirms our theoretical predictions. Note that for both elastomers based on the U1440 matrix, the relative damping factor is almost constant, which means that within a given time period, the amplitude of vibrations vanishes by a similar amount either with the magnets or without them, so the damping turns out to be ineffective. It is only the character of the oscillations that changes: the cycles are longer and their decrement is higher.

5.3. Effect of the Attached Mass. The additional mass of the magnets affects the dynamics of the system. The period of vibrations increases and the damping decrement is lower. On the other hand, the magnetic field generated by the magnets exerts the opposite effect, because it stiffens the damping block and increases its loss modulus. To analyze these effects separately, we apply the proposed mathematical model with the parameters the same as in experiments. The damping element is assumed to be made of MRE 1A which turned out to be the most sensitive to changing the magnetic field of all of the tested materials. Figure 12 compares the numerically obtained tip deflections of the beam without the magnet, with an artificial mass equal to the mass of the magnet and with the 5 mm neodymium magnet. Note that the strong field of the permanent magnet overcomes the negative effect of its additional mass. Still, such a positive relation of the magnetic field intensity to the mass is difficult to be obtained using electromagnets.

5.4. Compression of the Elastomers. When magnets are attached to the structure, they pull each other and squeeze the damping element. This introduces an additional stress, which may be expected to have an influence on the dynamics of the system. To analyze this effect, we inserted a plate at one side of the damping block (see Figure 13). Brass was chosen as the material of the plate because it does not modify the distribution of the magnetic field passing through the structure.

A comparison is shown in Figure 14. The compression of the elastomers increased their shear stiffness because the vibration period of the structure was shorter for the system without the plate than with the plate. This effect was observed in all of the analyzed scenarios. As could be expected, it was most pronounced for softest, MRE 1A.

5.5. Alignment of the Magnets. The magnets align themselves along the lines of the magnetic field to achieve the configuration of the lowest possible energy (Figure 15). This

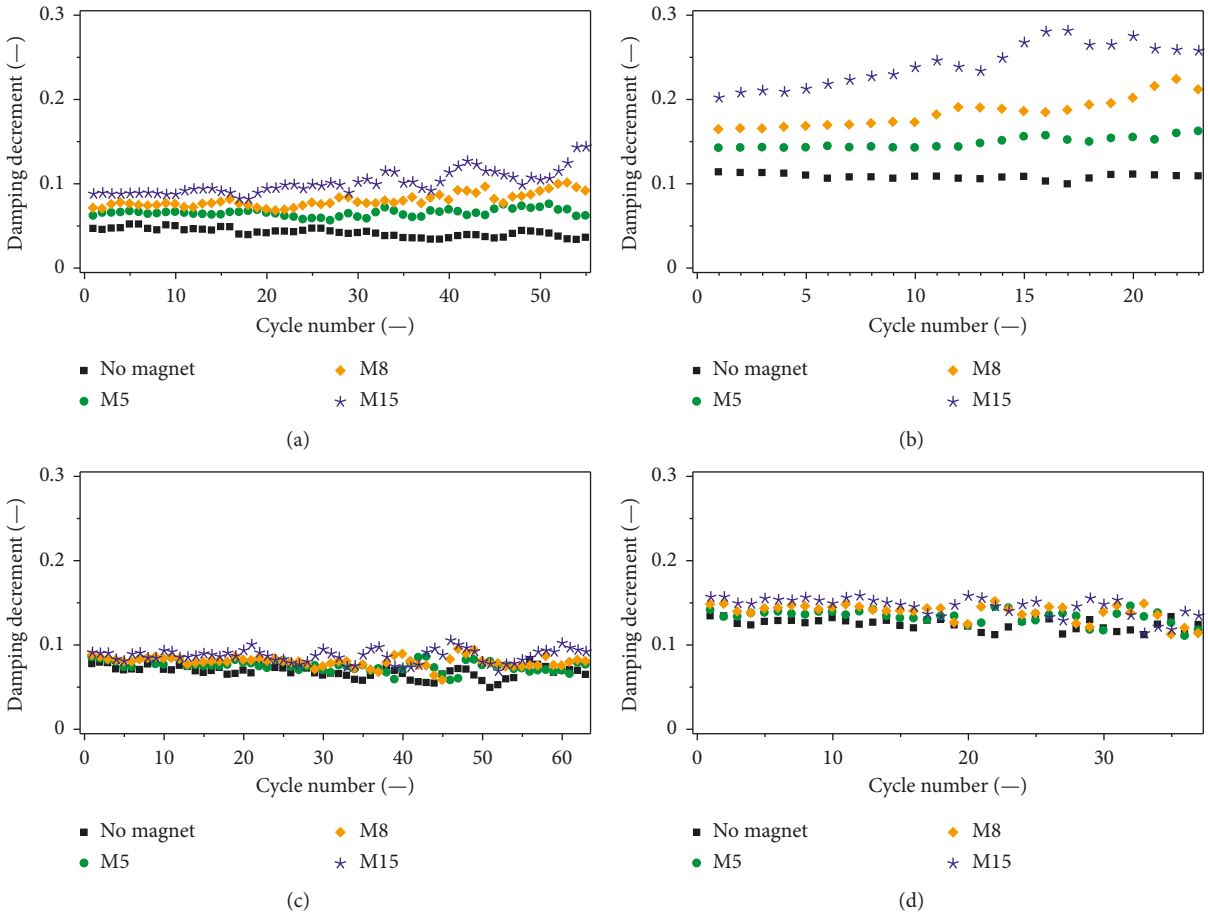

Figure 10: Logarithmic damping decrement of subsequent cycles: (a) MRE 1A, (b) MRE 1B, (c) MRE 2A, and (d) MRE 2B.

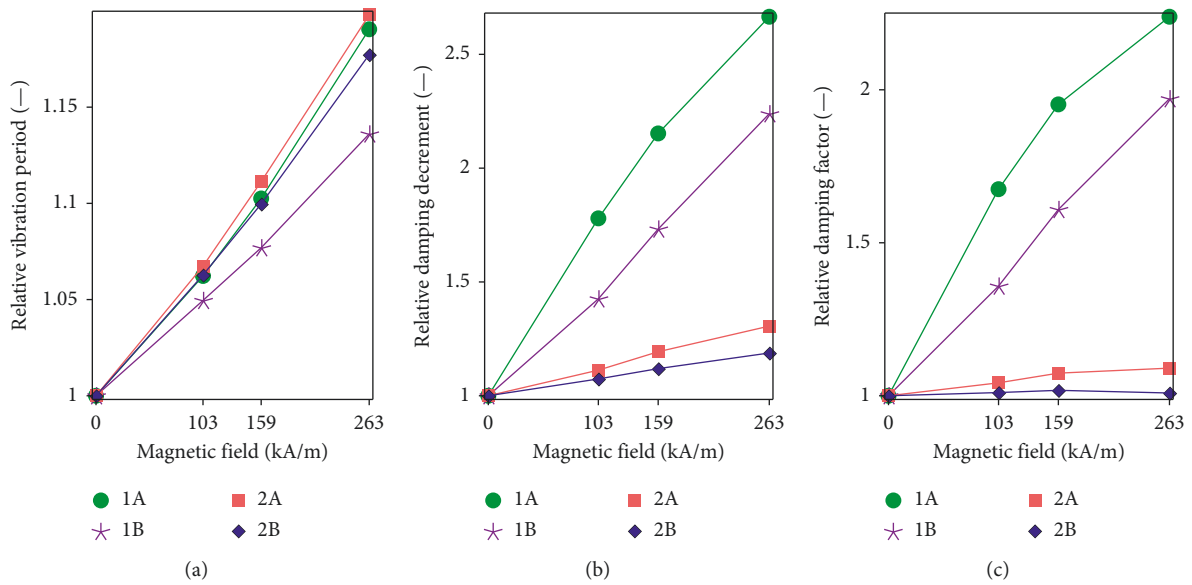

Figure 11: Relative increase of empirical vibration period (a), decrement (b), and damping ratio (c) for magnets M5 (103 kA/m), M8 (159 kA/m), and M15 (263 kA/m).

introduces an additional stiffness to the system. To analyze this effect, two brass rolls were placed between the M15 magnet and the beam, in two directions (Figure 16). When the rolls were inserted vertically, the magnet could align its position with the magnetic field. When they were in the horizontal position, this motion was prevented.

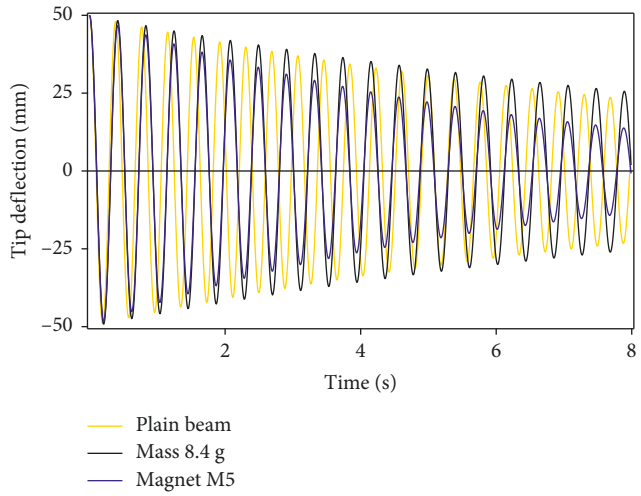

Figure 12: Tip deflection of the beam without the magnet (gold), with an artificial mass equal to the mass of the magnet (black) and with the 5 mm neodymium magnet (blue); MRE 1A.

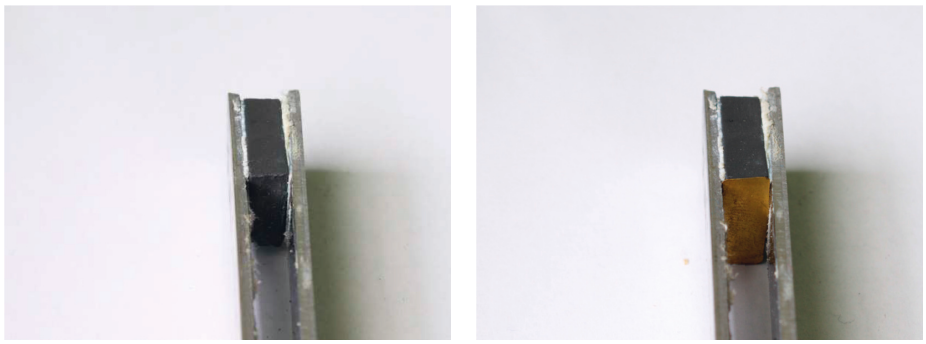

Figure 13: The brass plate to prevent compression of the elastomer.

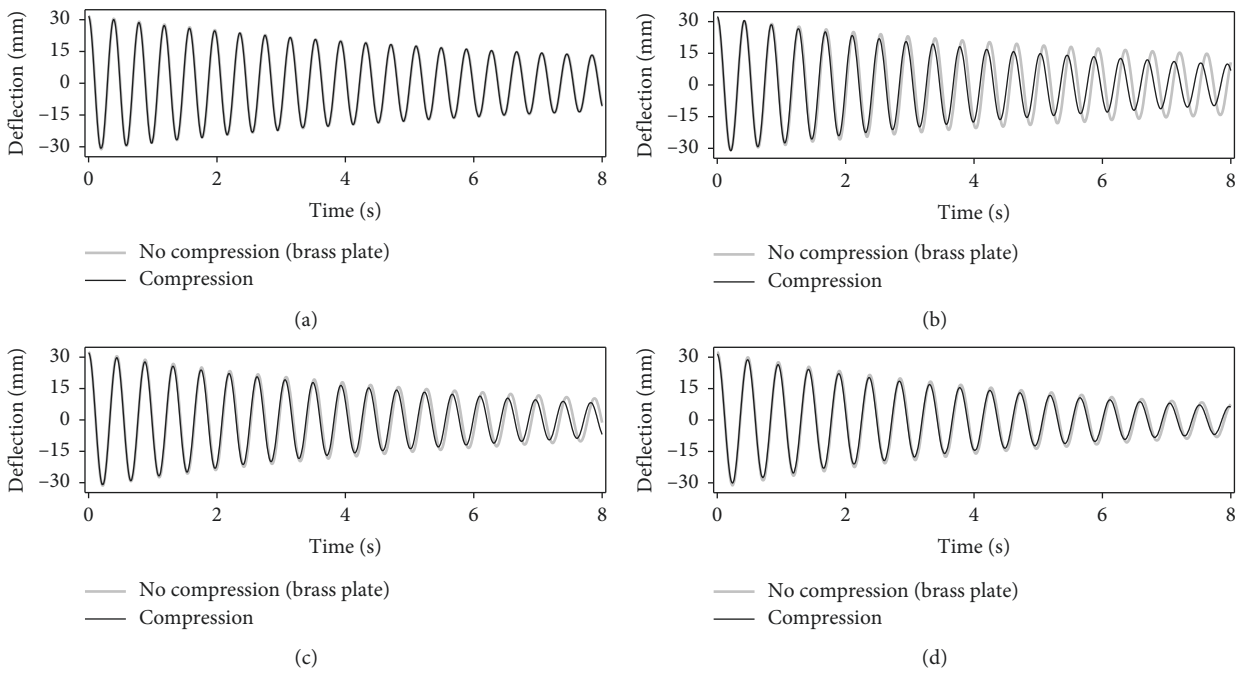

Figure 14: The effect of squeezing of the damping element MRE 1A: (a) no magnets, (b) magnets M5, (c) magnets M8, and (d) magnets M15.

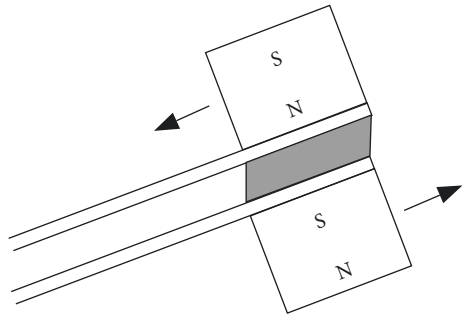

Figure 15: Alignment of magnets with the magnetic field.

(a) (b)

Figure 16: The rolls placed in two directions to analyze the effect of alignment of the magnets.

Although the motion of the magnet was hardly visible—which is understandable given that the shear strains were very low—the effect of rolling was observable, especially for the thin double-beam structure, in which the magnetic force between the magnets was higher than for the 6 mm thick structure (Figure 17).

6. Experimental Assessment of the Semiactive Control Strategy

6.1. Test Stand. To determine the additional functionality of the considered MRC blocks, associated with the increase in damping efficiency by applying a semiactive control strategy, an experimental investigation was carried out. For this purpose, the test stand described previously was modified. Similarly to the previous test rig (Figure 6), the ends of the two steel beams were supported with mounting brackets, and the MRE 1A element was glued at the free ends of the beams (see Figure 17). The MRE 1A block was selected because of all of the tested materials, it was the softest and the most sensitive to changing the magnetic field. This support enables horizontal displacements of the beams during the tests. In this investigation, the horizontal displacements were measured by the same laser displacement sensors OADM 12I6430/S35A. Here, four sensors in two pairs were set (see Figure 18). Each pair was used to estimate the horizontal displacement of the measuring point located between the two sensors. For this estimate, we used the average value measured by the two sensors, which allows an efficient signal filtering.

An electromagnet (GTo-30-0.5000-24VDC) was attached near the MRE 1A element, at the end of the beam structure. This electromagnet was mounted using the MS-polymer adhesive. To direct the magnetic flux beam generated by the electromagnet perpendicularly to the MRE block, on the opposite side of the steel beam, a neodymium magnet with dimensions of $10 \times 10 \times 3$ mm was used. The electromagnet was connected with the control unit by a current source, generating a control current proportional to a voltage signal that regulated a magnetic flux surrounded by the MRE block. The use of the current source allowed us to increase the rate of change of the magnetic flux generated by the magnet.

The electromagnet was turned on and off by a computer equipped with the semiactive control algorithm (20). The MRE block semiactive control strategy algorithm was adapted in the MATLAB environment, which was used to communicate with the measurement and control devices. For the tests, a National Instrument PCI 6251 analog-digital converter was used for data acquisition and control. All of the signals from the laser sensors were recorded by means of this converter with a sampling frequency of 1000 Hz. These signals provided information to the algorithm, which generated the control signal to the electromagnet with a sampling frequency of 50 Hz. The scheme of the measuring/control system is presented in Figure 19. The detailed parameters of the test stand (see Figure 18) used in the investigations are listed in Table 4.

6.2. Free Vibration Control Test. We aim at demonstrating the general performance of the selected MRE 1A block in

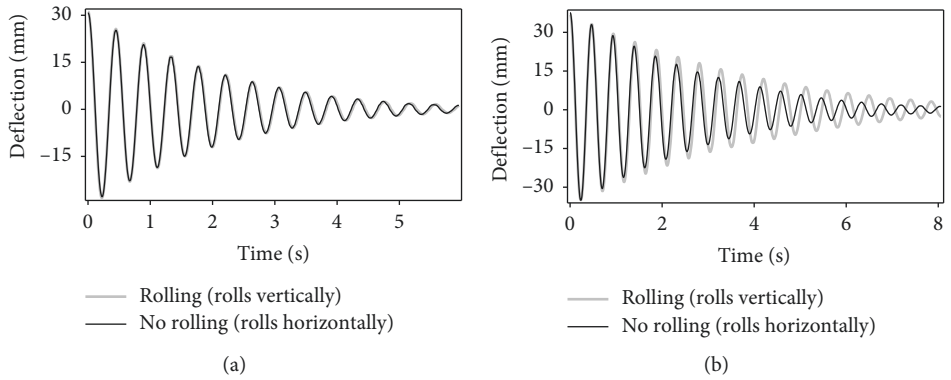

Figure 17: The effect of alignment of the magnets for the thick (6 mm (a)) and thin (4 mm (b)) structure, MRE 1B, magnets M15.

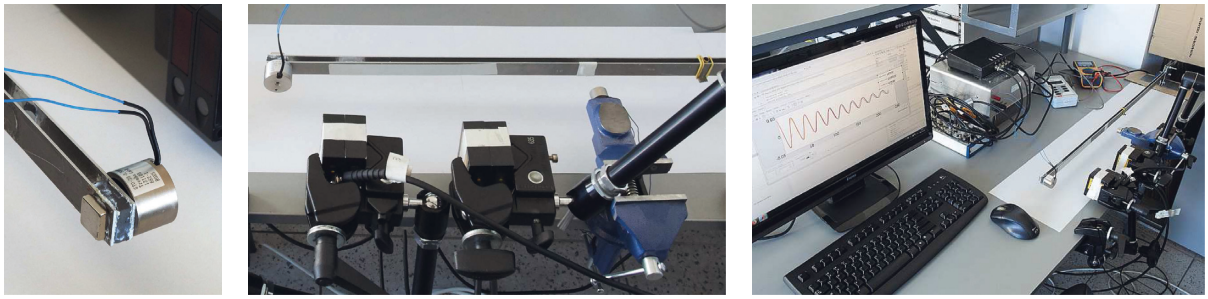

Figure 18: The test stand for the investigation of the control applied to the MRE element.

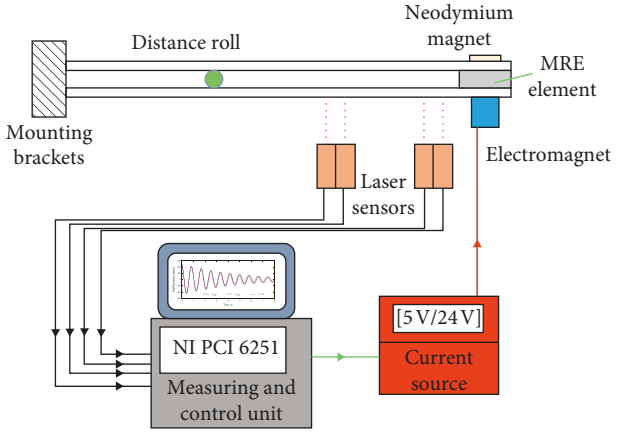

Figure 19: Diagram of the state-feedback control system.

mitigating the structural vibration. Therefore, in the present work, rather than performing a comprehensive control analysis, we limit our attention to the most typical cases of free vibration, where the deflections of the cantilever structure are concerned with the shape of its first natural mode W_1, as defined in (13). For this purpose, we carried out control experiments assuming the following initial state condition: $w_{1,2}(\xi, 0) = 50W_1(\xi)/W_1(L)$ (mm). As in the foregoing experiments, we selected the observation time to be $t_f = 8$ (s).

The state-feedback switched controller (20) relies on the measurements of two displacements $w_1(0.5(\xi_{s1} + \xi_{s2}), t)$ and $w_1(0.5(\xi_{s3} + \xi_{s4}), t)$ estimated by the two pairs of the laser sensors. These two measurements have been used to reconstruct the generalized coordinates $T_1^1(t)$ and $T_2^1(t)$ by using (12) and (13). For simplicity, we assume $w_2(0.5(\xi_{s1} + \xi_{s2}), t) = w_1(0.5(\xi_{s1} + \xi_{s2}), t)$ and $w_2(0.5(\xi_{s3} + \xi_{s4}), t) = w_1(0.5(\xi_{s3} + \xi_{s4}), t)$, and consequently $T_1^2(t) = T_1^1(t)$ and $T_2^2(t) = T_2^1(t)$. In order to justify the effectiveness of the semiactive controller, we will use the following functional as the stabilizing performance measure:

$$J(u) = \int_0^{t_f} V(t)dt, \tag{22}$$

where V is the total energy function defined as in (11). The performance of the control $u = u^*$ will be examined by comparison to the worst and the best passive cases, where we assume the extreme admissible control values $u = u_{\min}$

Table 4: Fundamental parameters of the second test stand.

Parameter	Value
Parameters of beam material (dural)	$\rho = 2.7$ g/cm^3, $E = 69$ GPa, $E^* = 40.3$ MPa·s
Dimensions of a single beam	$L = 860$, $b = 20$, $d = 1.6$ mm
Position of distance rolls	$x_1 = 350$ mm
Position of sensors from the support	$\xi_{s1} = 470$, $\xi_{s2} = 475$, $\xi_{s3} = 530$, $\xi_{s4} = 535$ mm
Dimensions of MRE blocks	$2a = 20$, $b = 20$, $2h = 6$ mm
Mass of MRE block	2 M = 4.4 g
Relative increase of G' and G'' under the field	$r_1 = 0.12$, $r_2 = 0.18$

(obtained for the voltage of 0 V) and $u = u_{\max}$ (obtained for the voltage of 24 V), respectively. The values of the objective functional (22) in the passive and the switched control cases are listed in Table 5. Each value is normalized to the passive case $u = u_{\min}$.

The comparison of the deflection of the end point of the lower beam $w_1(L,t)$ for the considered cases is depicted in Figure 20(a). Regarding the overall stabilizing performance, the reader can verify that the switched control (Figure 20(b)) provides better results than both passive damping strategies. In terms of the assumed functional (22), the control outperforms the worst and best passive cases by 13.2% and 7.6%, respectively. Comparing the last extreme deflections at $t \approx 7.3$ (s), the control results in a reduction of the vibration amplitude of 12.8% and 9.2%, respectively.

Table 5: The values of the objective function in the passive and the switched control cases.

	$u = u_{\min}$	$u = u_{\max}$	$u = u^*$
$J(u)(\cdot)$	1.000	0.939	0.868

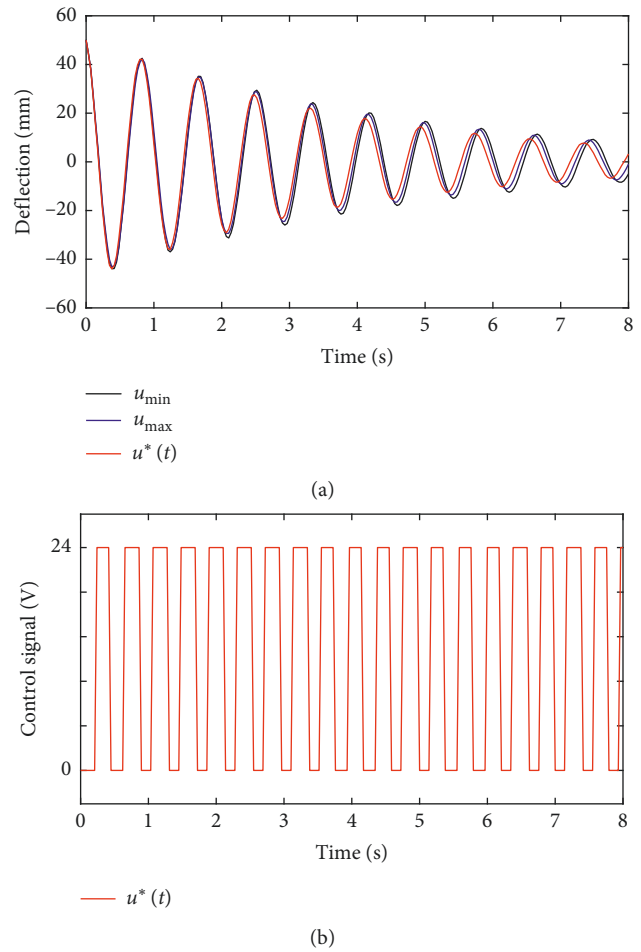

Figure 20: The trajectories of the tip deflection in the passive and the switched control cases (a) and switched control signal (b).

7. Conclusions

The use of magnetorheological elastomers for the mitigation of the free vibrations of a double-beam structure was studied. Four MREs with two types of polymeric matrices and two volume shares of iron particles were manufactured and tested on a rheometer to assess their storage and loss moduli within a magnetic field. Then, damping elements made of these materials were fabricated and glued between two cantilever beams, so that they coupled the free ends of the beams. The free vibrations of the first mode were induced and analyzed, and a simple linear model of the structure was developed. Both theoretical and experimental studies showed that the performance of the investigated method depends markedly on the type of the material and the permanent magnets attached:

(i) The PU 70/30 polymeric matrix is characterized by lower storage and loss moduli than the U1440 matrix, so its damping capabilities are not as good as the latter when no magnetic field is applied.

(ii) The magnetorheological effect for the PU 70/30 polymeric matrix is much more visible than for the U1440 matrix, which allows easier control of the damper. When a sufficiently strong magnetic field is applied, the storage and loss moduli of MREs based on the first type of matrix exceed those for the U1440-based elastomers.

(iii) Magnetorheological elastomers having 33 vol.% Fe provide higher stiffness, damping, and magnetorheological effects than those containing 11.5 vol.% of iron particles.

(iv) MRE 1B (PU 70/30, 33 vol.% Fe) was the most effective for vibration suppression of the investigated structure. We think that this is due to the unique microstructure and microstresses inside this material, which were obtained due to the selection of the properties of the components of this composite.

(v) The compression of the elastomers under the action of the magnetic forces, as well as the effect of the alignment of the magnets with the magnetic field, increases the stiffness and damping of the damping members.

(vi) Application of an elastomeric damping member at the end of the structure results in a sigmoidal shape of the first mode, so additional elements are necessarily along the structure to prevent buckling deformation.

(vii) The proposed model is very simple but it accurately captures the dynamics of the structure and allows development of the control strategy.

Data Availability

The data used to support the findings of this study are included within the article.

Conflicts of Interest

The authors declare that they have no conflicts of interest.

Acknowledgments

This research was supported by the National Science Centre, Poland, under grant agreements DEC-2013/11/D/ST8/03437, DEC-2015/17/D/ST8/02434, DEC-2017/25/B/ST8/01800, and DEC-2017/26/D/ST8/00883 and by the Polish National Centre for Research and Development, Poland, under Grant no. PBS1/A5/5/2012.

References

[1] T. Szmidt, D. Pisarski, C. Bajer, and B. Dyniewicz, "Double-beam cantilever structure with embedded intelligent damping block: dynamics and control," *Journal of Sound and Vibration*, vol. 401, pp. 127–138, 2017.

[2] F. Zhang, W. Liu, H. Fang, and Z. Jia, "Flexural behavior of composite sandwich beams with different kinds of gfrp ribs in flatwise and edgewise positions," *Composites Part B: Engineering*, vol. 156, pp. 229–239, 2019.

[3] H. Guoliang, G. Miao, W. Li, H. Du, and A. Gursel, "Experimental investigation of the vibration characteristics of a magnetorheological elastomer sandwich beam under non-homogeneous small magnetic fields," *Smart Materials and Structures*, vol. 20, no. 12, article 127001, 2011.

[4] F. Han, D. Dan, and W. Cheng, "Exact dynamic characteristic analysis of a double-beam system interconnected by a viscoelastic layer," *Composites Part B: Engineering*, vol. 163, pp. 272–281, 2019.

[5] J. Kozlowska, A. Boczkowska, A. Czulak et al., "Novel MRE/CFRP sandwich structures for adaptive vibration control," *Smart Materials and Structures*, vol. 25, no. 3, article 035025, 2016.

[6] V. Lara-Prieto, R. Parkin, M. Jackson, V. Silberschmidt, and Z. Kęsy, "Vibration characteristics of mr cantilever sandwich beams: experimental study," *Smart Materials and Structures*, vol. 19, no. 1, article 015005, 2010.

[7] S. Megha, S. Kumar, and R. D'Silva, "Vibration analysis of magnetorheological elastomer sandwich beam under different magnetic fields," *International Journal of Vehicle Design (IJVD)*, vol. 6, pp. 75–80, 2016.

[8] D. Bodniewicz, J. Kaleta, and D. Lewandowski, "The fabrication and the identification of damping properties of magnetorheological composites for energy dissipation," *Composite Structures*, vol. 189, pp. 177–183, 2018.

[9] Q. Liu and A. Chattopadhyay, "Improved helicopter aeromechanical stability analysis using segmented constrained layer damping and hybrid optimization," *Journal of Intelligent Materials Systems and Structures*, vol. 11, no. 6, pp. 492–500, 2000.

[10] M. Khoo and C. Liu, "Micro magnetic silicone elastomer membrane actuator," *Sensors and Actuators A: Physical*, vol. 89, no. 3, pp. 259–266, 2001.

[11] S. S. Sun, J. Yang, H. X. Deng et al., "Horizontal vibration reduction of a seat suspension using negative changing stiffness magnetorheological elastomer isolators," *International Journal of Vehicle Design*, vol. 68, no. 1–3, pp. 104–118, 2015.

[12] C. Bajer, D. Pisarski, T. Szmidt, and B. Dyniewicz, "Intelligent damping layer under a plate subjected to a pair of masses moving in opposite directions," *Journal of Sound and Vibration*, vol. 394, pp. 333–347, 2017.

[13] R. Bogacz, W. Czyczuła, and R. Konowrocki, "Influence of sleepers shape and configuration on track-train dynamics," *Shock and Vibration*, vol. 2014, Article ID 393867, 7 pages, 2014.

[14] A. Lago, D. Trabucco, and A. Wood, "Alternative to damping devices," in *Damping Technologies for Tall Buildings*, pp. 1067–1105, Butterworth-Heinemann, Oxford, UK, 2019.

[15] R. Kornbluh, H. Prahlad, R. Pelrine, S. Stanford, M. Rosenthal, and P. von Guggenberg, "Rubber to rigid, clamped to undamped: toward composite materials with wide-range controllable stiffness and damping," in *Proceedings of the SPIE, Smart Structures and Materials 2004: Industrial and Commercial Applications of Smart Structures Technologies*, vol. 5388, pp. 372–386, San Diego, CA, USA, March 2004.

[16] A. Pregowska, R. Konowrocki, and T. Szolc, "On the semi-active control method for torsional vibrations in electro-mechanical systems by means of rotary actuators with a magneto-rheological fluid," *Journal of Theoretical and Applied Mechanics*, vol. 51, no. 4, pp. 979–992, 2013.

[17] M. Farshad and A. Benine, "Magnetoactive elastomer composites," *Polymer Testing*, vol. 23, no. 3, pp. 347–353, 2004.

[18] G. Y. Zhou, "Shear properties of a magnetorheological elastomer," *Smart Materials and Structures*, vol. 12, no. 1, pp. 139–146, 2003.

[19] M. R. Jolly, J. D. Carlson, B. C. Muñoz, and T. A. Bullions, "The magnetoviscoelastic response of elastomer composite consisting of ferrous particles embedded in a polymer matrix," *Journal of Intelligent Material Systems and Structures*, vol. 7, no. 6, pp. 613–622, 1996.

[20] J. M. Ginder, M. E. Nichols, L. E. Elie, and S. M. Clark, "Controllable-stiffness components based on magnetorheological elastomers," *Smart Structures and Smart Materials*, vol. 3985, 2000.

[21] J. Yao, Y. Sun, Y. Wang, Q. Fu, Z. Xiong, and Y. Liu, "Magnet-induced aligning magnetorheological elastomer based on ultra-soft matrix," *Composites Science and Technology*, vol. 162, pp. 170–179, 2018.

[22] F. de Souza Eloy, G. F. Gomes, A. C. Ancelotti, S. S. da Cunha, A. J. F. Bombard, and D. M. Junqueira, "A numerical-experimental dynamic analysis of composite sandwich beam with magnetorheological elastomer honeycomb core," *Composite Structures*, vol. 209, pp. 242–257, 2019.

[23] T. Komatsuzaki, T. Inoue, and O. Terashima, "Broadband vibration control of a structure by using a magnetorheological elastomer-based tuned dynamic absorber," *Mechatronics*, vol. 40, pp. 128–136, 2016.

[24] R. B. Vemuluri, V. Rajamohan, and P. E. Sudhagar, "Structural optimization of tapered composite sandwich plates partially treated with magnetorheological elastomers," *Composite Structures*, vol. 200, pp. 258–276, 2018.

[25] A. Boczkowska and S. F. Awietjan, "Effect of the microstructure on rheological properties of the urethane magnetorheological elastomers," in *Proceedings of the Mesomechanics 2008 HBRC*, vol. M29, p. 8, Giza, Egypt, January-February 2008.

[26] M. Lokander and B. Stenberg, "Improving the magnetorheological effect in isotropic magnetorheological rubber materials," *Polymer Testing*, vol. 22, no. 6, pp. 677–680, 2003.

[27] Y. An and M. T. Shaw, "Actuating properties of soft gels with ordered iron particles: basis for a shear actuator," *Smart Materials and Structures*, vol. 12, no. 2, pp. 157–163, 2003.

[28] A. Boczkowska, S. F. Awietjan, S. Pietrzko, and K. J. Kurzydłowski, "Mechanical properties of magnetorheological elastomers under shear deformation," *Composites Part B: Engineering*, vol. 43, no. 2, pp. 636–640, 2012.

[29] A. Allahverdizadeh, M. J. Mahjoob, M. Maleki, N. Nasrollahzadeh, and M. H. Naei, "Structural modeling, vibration analysis and optimal viscoelastic layer characterization of adaptive sandwich beams with electrorheological fluid core," *Mechanics Research Communications*, vol. 51, pp. 15–22, 2013.

[30] G. Y. Zhou and Q. Wang, "Use of magnetorheological elastomer in an adaptive sandwich beam with conductive skins. Part I: magnetoelastic loads in conductive skins," *International Journal of Solids and Structures*, vol. 43, no. 17, pp. 5386–5402, 2006.

[31] S. K. Dwivedy, N. Mahendra, and K. C. Sahu, "Parametric instability regions of a soft and magnetorheological elastomer cored sandwich beam," *Journal of Sound and Vibration*, vol. 325, no. 4-5, pp. 686–704, 2009.

[32] B. Nayak, S. K. Dwivedy, and K. Murthy, "Vibration analysis of a three-layer magnetorheological elastomer embedded sandwich beam with conductive skins using finite element method," *Proceedings of the Institution of Mechanical Engineers, Part C: Journal of Mechanical Engineering Science*, vol. 227, no. 4, pp. 714–729, 2013.

[33] E. Manjarekar, S. Kumbhar, and U. D. Gulhane, "Study and vibration response analysis of MR cantilever beam," *International Journal of Engineering Development and Research*, vol. 3, no. 1, pp. 288–293, 2014.

[34] B. Nayak, S. K. Dwivedy, and K. S. R. K. Murthy, "Dynamic analysis of magnetorheological elastomer-based sandwich beam with conductive skins under various boundary conditions," *Journal of Sound and Vibration*, vol. 330, no. 9, pp. 1837–1859, 2011.

[35] J.-Y Yeh, "Vibration analysis of sandwich rectangular plates with magnetorheological elastomer damping treatment," *Smart Materials and Structures*, vol. 22, no. 3, pp. 75–80, 2013.

[36] M. Ramamoorthy, V. Rajamohan, and J. Ak, "Vibration analysis of a partially treated laminated composite magnetorheological fluid sandwich plate," *Journal of Vibration and Control*, vol. 22, no. 3, pp. 869–895, 2016.

[37] B. P. Ndemanou, B. R. Nana Nbendjo, and U. Dorka, "Quenching of vibration modes on two interconnected buildings subjected to seismic loads using magneto rheological device," *Mechanics Research Communications*, vol. 78, pp. 6–12, 2016.

[38] D. Pisarski, T. Szmidt, C. I. Bajer, B. Dyniewicz, and J. M. Bajkowski, "Vibration control of double-beam system with multiple smart damping members," *Shock and Vibration*, vol. 2016, Article ID 2438902, 14 pages, 2016.

[39] V. Rajamohan, R. Sedaghati, and S. Rakheja, "Optimal vibration control of beams with total and partial mr fluid treatments," *Smart Materials and Structures*, vol. 20, no. 11, article 115016, 2011.

[40] B. Dyniewicz, J. M. Bajkowski, and C. I. Bajer, "Semi-active control of a sandwich beam partially filled with magnetorheological elastomer," *Mechanical Systems and Signal Processing*, vol. 60-61, pp. 695–705, 2015.

[41] A. Boczkowska and S. F. Awietjan, *Advanced Elastomers, Technology, Properties and Applications, Chapter Microstructure and Properties of Magnetorheological Elastomers*, Intech, Vienna, Austria, 2012.

[42] T. Szmidt, "Shear deformation damping of a double-beam structure," *Journal of Sound and Vibration*, vol. 370, pp. 163–175, 2016.

[43] D. Pisarski, "Decentralized stabilization of semi-active vibrating structures," *Mechanical Systems and Signal Processing*, vol. 100, pp. 694–705, 2018.

[44] R. Bogacz and R. Konowrocki, "On new effects of wheel-rail interaction," *Archive of Applied Mechanics*, vol. 82, no. 10-11, pp. 1313–1323, 2012.

[45] R. Konowrocki and C. I. Bajer, "Friction rolling with lateral slip in rail vehicles," *Journal of Theoretical and Applied Mechanics*, vol. 47, no. 2, pp. 275–293, 2009.